# Development of a Continuum Damage Mechanics Material Model of a Graphite-Kevlar® Hybrid Fabric for Simulating the Impact Response of Energy Absorbing Subfloor Concepts

**Karen E. Jackson**
Aerospace Engineer
NASA Langley Research Center
Hampton, VA, USA

**Edwin L. Fasanella**
Aerospace Engineer
National Institute of Aerospace
Hampton, VA, USA

**Justin D. Littell**
Aerospace Engineer
NASA Langley Research Center
Hampton, VA, USA

## ABSTRACT

This paper describes the development of input properties for a continuum damage mechanics based material model, Mat 58, within LS-DYNA® to simulate the response of a graphite-Kevlar® hybrid plain weave fabric. A limited set of material characterization tests were performed on the hybrid graphite-Kevlar® fabric. Simple finite element models were executed in LS-DYNA® to simulate the material characterization tests and to verify the Mat 58 material model. Once verified, the Mat 58 model was used in finite element models of two composite energy absorbers: a conical-shaped design, designated the "conusoid," fabricated of four layers of hybrid graphite-Kevlar® fabric; and, a sinusoidal-shaped foam sandwich design, designated the "sinusoid," fabricated of the same hybrid fabric face sheets with a foam core. Dynamic crush tests were performed on components of the two energy absorbers, which were designed to limit average vertical accelerations to 25- to 40-g, to minimize peak crush loads, and to generate relatively long crush stroke values under dynamic loading conditions. Finite element models of the two energy absorbers utilized the Mat 58 model that had been verified through material characterization testing. Excellent predictions of the dynamic crushing response were obtained.

## INTRODUCTION

In 2012, the NASA Rotary Wing Aeronautics Program sponsored the Transport Rotorcraft Airframe Crash Testbed (TRACT) research program in which two CH-46E Sea Knight helicopter airframes were crash tested at the Landing and Impact Research (LandIR) facility located at NASA Langley Research Center in Hampton, Virginia. The crash tests were conducted to assess dynamic responses of transport-category rotorcraft under combined forward and vertical impact loading. The CH-46E airframe is categorized as a medium-lift rotorcraft with length and width of 45- and 7-ft, respectively, and a capacity for 5 crew and 25 troops. The first crash test, TRACT 1 [1], was conducted in August 2013 under combined conditions of 300-in/s vertical and 396-in/s forward velocities onto a 2-ft.-deep soil bed, which is characterized as a sand/clay mixture. The primary objectives for TRACT 1 were to assess improvements in occupant loads and flail envelope with the use of crashworthy features such as pre-tensioning active restraints and load limiting seats and to develop novel techniques for photogrammetric data acquisition to measure occupant and airframe kinematics.

The TRACT 1 airframe was tested in a baseline configuration with no changes to the structural configuration, including the discrete aluminum shear panels in the subfloor. A final objective of TRACT 1 was to generate crash test data in a baseline configuration for comparison with data obtained from a similar TRACT 2 crash test.

A crash test of the second CH-46E airframe (TRACT 2) was conducted on October 1, 2014, and was performed for the same nominal impact velocity conditions and onto the same sand/clay surface [2]. Changes from the baseline TRACT 1 test article included replacement of two subfloor shear panels with NASA-developed composite energy absorbing subfloor concepts. A third corrugated web energy absorber, which was developed by the German Aerospace Research Center (DLR) and the Australian Cooperative Research Centre for Advanced Composite Structures (ACS-CRC), was also retrofitted into TRACT 2 [3, 4]. However, this concept will not be discussed in this paper. The two NASA concepts were located in the mid-cabin region and included a conical-shaped design, designated the "conusoid," fabricated of four layers of hybrid graphite-Kevlar® fabric [5]; and a sinusoidal-shaped foam sandwich design, designated the "sinusoid," fabricated of the same hybrid fabric face sheets with a foam core [6]. While the TRACT 2 airframe contained similar seat, occupant, and restraint experiments, major goals of the test were to evaluate the performance of novel composite energy absorbing subfloor designs for improved crashworthiness and to investigate the capabilities of LS-DYNA® to predict the impact response.

Presented at the AHS International 73rd Annual Forum & Technology Display, Fort Worth, Texas, USA, May 9-11, 2017.

Components of the conusoid and sinusoid energy absorbers are depicted in Figure 1. The design goals in developing these energy absorbers were to limit the average vertical accelerations to 25- to 40-g, to minimize peak crush loads, and to generate relatively long crush stroke values under dynamic loading conditions, typical of those experienced during the TRACT 1 full-scale crash test [1]. Note that crush stroke is defined as the crush displacement divided by the original height of the specimen and is often expressed as a percentage value.


(a) Conusoid component.

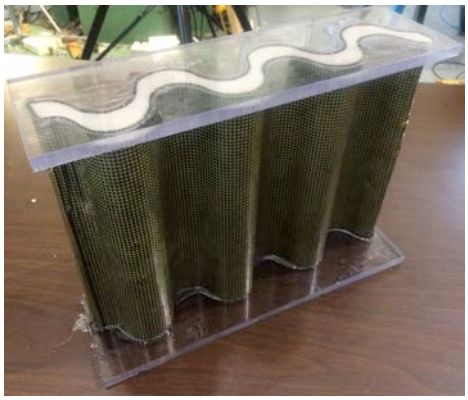

(b) Sinusoid component.

Figure 1. Photographs of two energy absorbers.

Finite element models were developed using the commercial, nonlinear explicit transient dynamic code, LS-DYNA® [7-9], to simulate the response of the conusoid and sinusoid energy absorbers [10]. One key to the success of the modeling effort was the development of an accurate material model of the hybrid graphite-Kevlar® fabric used in the construction of both energy absorbers. The hybrid graphite-Kevlar® fabric layers were assigned Mat 58, which is a continuum damage mechanics material model used in LS-DYNA® for representing composite laminates and fabrics [11]. Input property values for Mat 58 can be obtained from standard material characterization tests. Ideally, these tests would include tensile and compressive testing of fabric coupons oriented at 0°, 90°, and ±45° to obtain longitudinal stiffness and strength, transverse stiffness and strength, and shear stiffness and strength, respectively. For this project, a limited set of material characterization tests was performed. The Mat 58 properties were verified through comparison with coupon test data. It should be noted that Mat 58 includes certain parameters that cannot be determined entirely based on experimental data. For these parameters, estimates were input based on past experience of the analysts.

A close-up photograph of the hybrid graphite-Kevlar® plain weave fabric is shown in Figure 2, in which the graphite fibers are oriented vertically (warp direction) and the Kevlar® fibers are oriented horizontally (fill direction). Note that Mat 58 does not represent the individual fibers within a layer of fabric material, and, instead, represents each layer in the composite laminate with smeared properties.

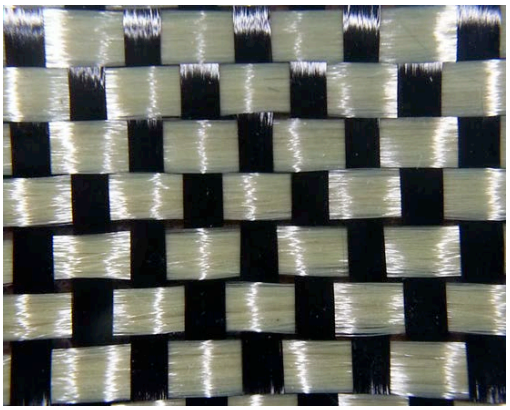

Figure 2. Hybrid graphite-Kevlar® plain weave fabric.

This paper will provide a description of Mat 58 and present material test data representing the response of the hybrid graphite-Kevlar® fabric material used in the construction of the two energy absorbers. In addition, analytical predictions of the material characterization tests will be shown to demonstrate how Mat 58 input values were derived. The Mat 58 material model was then assigned to shell elements in the finite element models of the energy absorbers, and the simulations were executed to predict dynamic crushing response. Test-analysis comparisons are presented for dynamic crush tests of each energy absorber.

## MATERIAL TESTING AND SIMULATION OF HYBRID GRAHITE-KEVLAR® FABRIC

A major challenge in developing a reliable and robust shell-based model of the two composite energy absorbers is to generate an accurate material model to represent the hybrid graphite-Kevlar® fabric used in their construction. The use of multi-layered shell elements in modeling the thin composite structure provides for a more realistic representation of the actual geometry than can be generated using solid elements. In addition, material property degradation of individual plies can be implemented based on damage mechanics models. However, modeling of composites has long been complicated by the variety of failure modes they exhibit under compressive loading, such as local buckling, delamination, and tearing. These

interacting failure modes can complicate the ability to simulate the crush response of the energy absorbers under load. To accurately characterize the hybrid graphite-Kevlar® fabric, an LS-DYNA® material model was needed with the capability to predict the observed failure mechanisms and to demonstrate good functionality when used in conjunction with a shell-element-based model.

Many different composite materials and layup combinations were evaluated as potential candidates for the energy absorbers. Specific interest was given to both conventional and hybrid families of woven fabrics [5]. Hybrid material systems consisting of graphite and aramid fibers were considered for use as they have exhibited desirable energy absorption characteristics in the past. For example, Farley [12] has shown that high values of specific sustained crush stress are obtained during dynamic crush tests of hybrid graphite-Kevlar® composite tubes in which the graphite fibers are oriented in the same direction as the loading axis and the Kevlar fibers are oriented at ±45° to the loading axis. As stated in Reference 12, "the Kevlar fibers are positioned in the laminate to provide containment and support for the graphite fibers, which absorb energy through a combination of crushing and fracturing modes."

**Mat 58 Laminated Composite Fabric Material Model**

The Mat 58 material model was initially chosen as a result of past success in predicting debris impact damage to the Reinforced Carbon-Carbon leading edge panels of the Space Shuttle Columbia [13]. Mat 58 is a continuum damage mechanics material model based on the theory described in Reference 11 and is intended for use with shell elements to simulate composite tape laminates and woven fabrics. Reference 14 describes the implementation of Mat 58 within LS-DYNA®. The model requires input of material properties in tension, compression, and shear to define stress-strain behavior within the lamina or laminate. The user specifies the in-plane elastic moduli in two primary directions, designated A (typically used for the longitudinal or fiber direction) and B (typically used for the transverse or perpendicular-to-the-fiber direction) in LS-DYNA®. The maximum strength values in tension, compression, and shear are also specified at corresponding strain values.

A representation of the stress-strain curve for in-plane tension is illustrated in Figure 3. The tensile response is initially linear elastic with the modulus specified by EA. Stress increases nonlinearly until XT, the maximum strength, is reached, which also corresponds to the strain at the longitudinal strength, E11T. The nonlinear portion of the response is defined internally by LS-DYNA® based on a continuum damage approach. Once XT is reached, the stress is reduced based on the "stress limiting" factor, SLIMT1, and is then held constant at the reduced value until a strain specified by the ERODS parameter is reached, at which point the individual ply within the composite laminate is removed. Mat 58 properties used in the current modeling effort to represent hybrid graphite-Kevlar® fabric material are listed in Table 1.

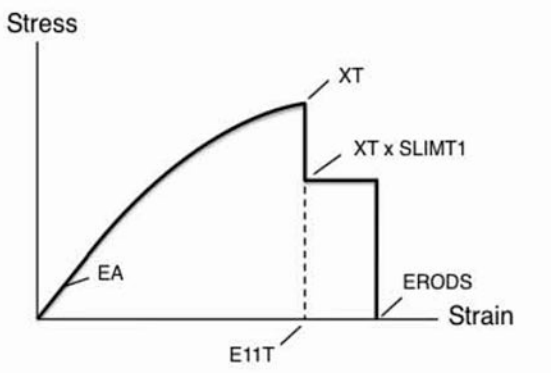


Figure 3. Typical in-plane tension stress-strain curve used in Mat 58 [7, 8].

**Table 1. Mat 58 Material Properties for Hybrid Fabric.**

| Material Property Description | Symbol | Value |
|---|---|---|
| Density, lb-s$^2$/in$^4$ | RO | 1.29E-4 |
| Longitudinal Young's modulus, psi | EA | 6.3E+6 |
| Transverse Young's modulus, psi | EB | 2.76E+6 |
| Poisson's ratio, $\nu_{BA}$ | PRBA | 0.1095 |
| Stress limit of nonlinear portion of the shear curve, psi | TAU1 | 4,500. |
| Strain limit of nonlinear portion of the shear curve, in/in | GAMMA1 | 0.0246 |
| Shear moduli, psi | GAB | 3.0E+5 |
| Min stress factor for limit after max stress (fiber tension) | SLIMT1 | 0.8 |
| Min stress factor for limit after max stress (fiber comp) | SLIMC1 | 1.0 |
| Min stress factor for limit after max stress (matrix tension) | SLIMT2 | 0.8 |
| Min stress factor for limit after max stress (matrix comp) | SLIMC2 | 1.0 |
| Min stress factor for limit after max stress (shear) | SLIMS | 1.0 |
| Material axes option | AOPT | 2.0 |
| Max strain for layer failure | ERODS | 0.5 |
| Failure surface type | FS | -1.0 |
| Components of **a** for AOPT = 2 | A1, A2, A3 | |
| Components of **d** for AOPT = 2 | D1, D2, D3 | |
| Strain at longitudinal compressive strength, in/in | E11C | 0.013 |
| Strain at longitudinal tensile strength, in/in | E11T | 0.0143 |
| Strain at transverse compressive (comp) strength, in/in | E22C | 0.025 |
| Strain at transverse tensile strength, in/in | E22T | 0.025 |
| Strain at shear strength, in/in | GMS | 0.142 |
| Longitudinal comp strength, psi | XC | 70,000. |
| Longitudinal tensile strength, psi | XT | 89,000. |
| Transverse comp strength, psi | YC | 50,000. |
| Transverse tensile strength, psi | YT | 54,000. |
| Shear strength, psi | SC | 7,100. |

Mat 58 includes several parameters that need additional clarification. The first parameter is PRBA, which is the

Poisson's ratio in the BA direction, $\nu_{BA}$. PRBA is considered the minor Poisson's ratio. This parameter is somewhat unusual in that most composite material models require input of $\nu_{AB}$, which is the major Poisson's ratio. A second parameter is AOPT, which is used to define the material direction. For composite materials, this parameter is especially important. As listed in Table 1, AOPT is set to 2.0, which means that the material direction is determined based on the cross product of two vectors, **a** x **d**. For the 0° loading case, the vectors are chosen such that the primary material direction is aligned with the global x-axis. For the 90° loading case, the vectors are chosen such that the primary material direction is aligned with the global y-axis. Finally, for the ±45° loading case, the vectors are chosen such that the primary material direction is oriented at ±45° with respect to the global x-axis. The third parameter of interest is FS, which specifies the failure surface used in the simulation. Three options are available (FS = 1.0, FS = 0.0, and FS = -1.0). For the simulations described herein, a value of -1.0 was selected indicating a faceted failure surface. For this failure surface, damage evolves independently in tension, compression, and shear for both the fiber and transverse directions [8, 9]. For fabric materials, a nonlinear shear stress versus shear strain curve is assumed when FS = -1.0, as depicted in Figure 4. This option is not available for other FS types. The final parameter is ERODS, which defines the maximum effective strain for element layer failure. Typically, the value of ERODS is set fairly high. For example, ERODS = 0.5 in this simulation study, which means that element layers cannot be removed, or eroded, until the effective strain is 50%. If the erosion parameter is set too low, holes produced in the model by element deletion could lead to premature failure and unstable model behavior.

As shown in Figure 4, the shear stress versus strain response is assumed to be nonlinear, following a brief linear elastic region defined by the shear modulus, GAB. With FS = -1.0, additional inputs are required to Mat 58 including the strain (GAMMA1) at the initial nonlinear portion of the response and the corresponding stress (TAU1). These parameters are somewhat nebulous, and are selected based on the experience of the analyst. However, the shear strain (GMS) and the maximum shear strength (SC) can be determined from test data. The parameter SLIMS is used to reduce the stress, once SC is achieved. This stress level is maintained until the strain parameter ERODS is reached.

It should also be noted that Mat 58 does not require input of compressive stiffness properties. Thus, it is assumed that the compressive moduli are equal to the tension values, indicating that Mat 58 cannot replicate bimodular elastic behavior. However, failure in compression can be different than failure in tension, based on the input values of E11C, the value of strain at the longitudinal compressive strength; E22C, the value of strain at the transverse compressive strength; XC, the longitudinal compressive strength; and YC, the transverse compressive strength. Since no compressive material tests were performed, these values were determined based on manufacturer's data.

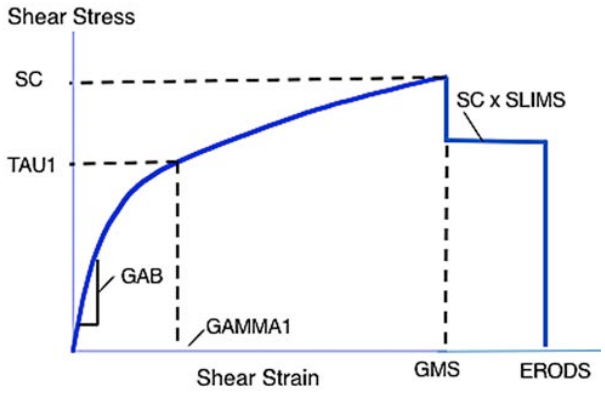


Figure 4. Schematic of nonlinear shear stress versus strain response with FS = -1.0 [7-9].

Material Characterization Testing

As mentioned previously, a limited set of material characterization tests were performed on the hybrid graphite-Kevlar® fabric, including tensile tests of coupons in which the graphite fibers were oriented in the 0° longitudinal (axial) direction, tensile tests of coupons in which the graphite fibers were oriented in the 90° transverse direction, and tensile tests of coupons in which the graphite fibers were oriented in a ±45° direction. These tests were performed on 10-in. x 1-in. coupons with a gauge length of 6-in., and a 4-ply stacking sequence, with total thickness of approximately 0.04-in. Tensile tests were conducted in accordance with ASTM 3039 [15], and in-plane shear tests were conducted in accordance with ASTM 3518 [16].

The longitudinal tensile stress versus strain is plotted in Figure 5, which represents the average response obtained from three repeated tests of coupons in which the graphite fibers are oriented at 0° with respect to the axial direction. Stress was determined by dividing the measured load, recorded on a MTS load-test machine, by the cross-sectional area of the specimen. Strain was determined at three locations along the length of the gauge section using digital image correlation in conjunction with a speckle pattern that was sprayed onto the specimen. The three strain measurements were averaged for each test. The following material properties were obtained: Young's modulus in the longitudinal direction (EA) = 6.3E+06 psi, longitudinal tensile strength (XT) = 89,000 psi, and longitudinal tensile strain at the tensile strength (E11T) = 0.0143 in/in. These values were input to Mat 58, as shown in Table 1.

Test results are plotted in Figure 6 for transverse tensile stress versus strain from coupons in which the graphite fibers are oriented at 90° with respect to the axial direction. Two coupon responses were averaged to obtain the response shown in Figure 6. Based on this data, the following values were determined: Young's modulus in the transverse direction (EB) = 2.76E+06 psi, transverse tensile strength

(YT) = 54,000 psi, and the transverse tensile strain at the tensile strength (E22T) = 0.025 in/in. These values were input to Mat 58, as shown in Table 1.

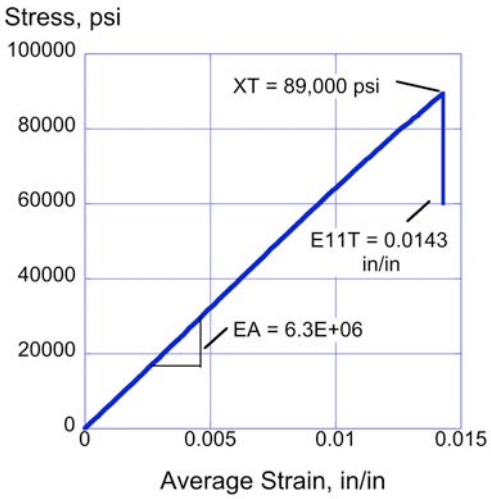


Figure 5. Stress vs. average strain for 0° specimens.

Average test results are plotted in Figure 7(a) for two coupons in which the graphite fibers are oriented at ±45° with respect to the axial direction. This test is used to derive shear properties of the material. Shear stress is determined by dividing the measured axial stress by 2. Shear strain is equal to the sum of the axial and transverse strains, $\gamma_{xy} = (\varepsilon_x + \varepsilon_y)$. However, since the transverse strain was not measured, then $\gamma_{xy} = \varepsilon_x + \varepsilon_y = \varepsilon_x - \nu_{xy}\varepsilon_x = \varepsilon_x(1 - \nu_{xy})$. Assuming $\nu_{xy} = 0.25$, then $\gamma_{xy} = 0.75\varepsilon_x$. The data shown in Figure 7(a) were converted to shear stress versus shear strain and are plotted in Figure 7(b). Several material parameters were determined based on the data shown in Figure 7(b) including: shear modulus (GAB) = 3.0E+05 psi, shear strain (GMS) = 0.142 in/in, shear strength (SC) = 7,100 psi, the stress limit of the nonlinear portion of the shear curve (TAU1) = 4,500 psi, and the strain limit of the nonlinear portion of the shear curve (GAMMA1) = 0.0246 in/in. These values were input to Mat 58, as shown in Table 1.

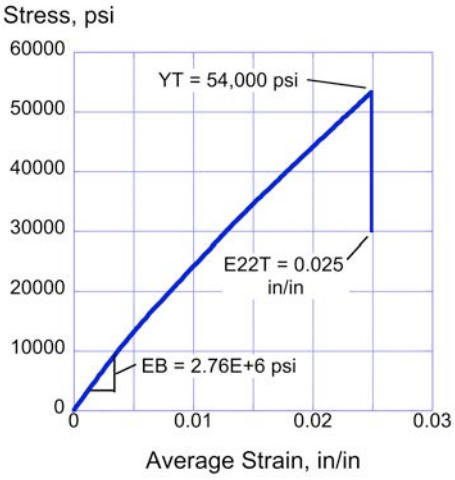


Figure 6. Stress vs. average strain for two 90° coupons.

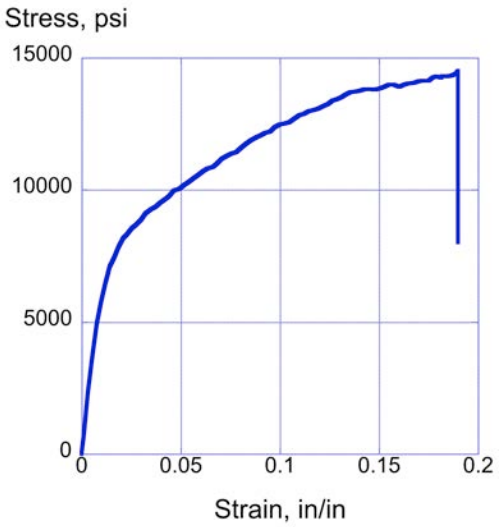


(a) Test results.

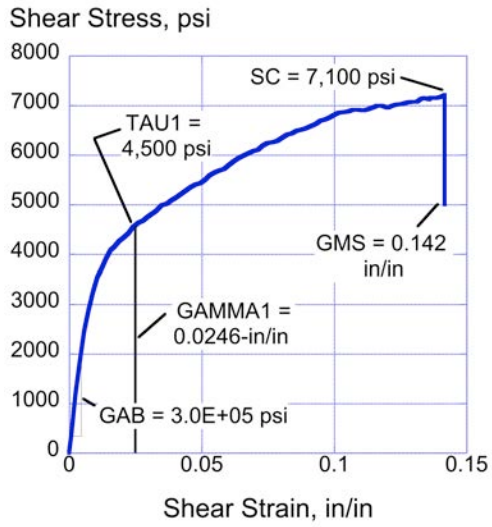


(b) Computed shear stress versus shear strain.

Figure 7. Stress versus average strain for ±45° specimens.

LS-DYNA® Modeling of the Material Tests

A simple finite element model was developed and executed to simulate the material characterization tests previously described. Instead of simulating the actual 1-in. x 6-in. gauge section of the coupon, a 1-in. x 1-in. model was developed, which provided a more uniform stress distribution across the width of the specimen. The model, shown in Figure 8, contained 289 Belytschko-Tsay shell elements, 329 nodes, 1 material property (Mat 58), and 1 part definition. Four layers were input using the *PART_COMPOSITE feature in LS-DYNA which allows the user to assign ply thickness, orientation, and material property for each layer in the composite. A Single Point Constraint (SPC) was defined to fix the nodes on the left side of the model. In addition, the nodes on the right side of the model were assigned a boundary prescribed motion card

such that, at the start time, the displacement in the x-direction was zero and at the end time (0.3-seconds) it was 0.05-in. The model was loaded slowly to minimize the kinetic energy of the simulation, thus recreating the quasi-static conditions used during the test. Output from the model included the SPC force at each node on the left side of the model. These forces were summed and divided by the cross-sectional area of the specimen to obtain stress. Strain was derived as a ratio of the time and displacement and was divided by the original length (1-in.) of the specimen.

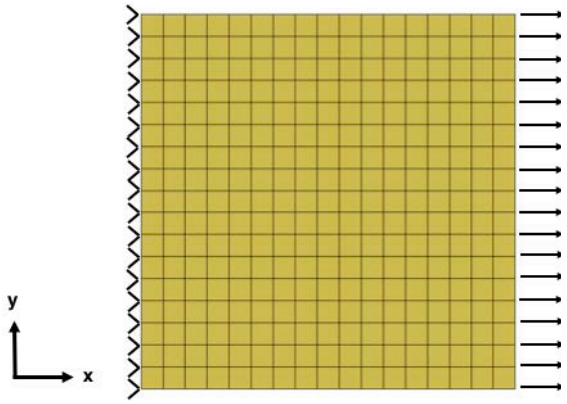


Figure 8. Finite element model used for material property comparisons.

Test-Analysis Comparisons of Material Tests

Plots of test-analysis comparisons are shown in Figures 9-11 for the 0° longitudinal tensile loading case, the 90° transverse tensile loading case, and the ±45° shear loading case, respectively. For the longitudinal 0° loading case, shown in Figure 9, the model accurately predicted the linear elastic portion of the test response. At a stress of approximately 79,000 psi, the predicted load response dropped off, likely due to transverse yielding occurring in one or more plies. The stress increases following this initial drop and achieves a maximum value of 80,000 psi. The predicted maximum strength occurs at a strain of 0.016 in/in. For this simulation, the value of SLIMT1 was lowered from 0.8 to 0.2 to mimic the observed response. As shown in the plot, the parameter SLIMT1 has lowered the predicted maximum stress to approximately 20% of its original value. This stress level will be maintained until the value of ERODS is reached. The test response is linear to failure, which occurs at a stress value of 89,000 psi and a strain of 0.0143 in/in.

For the transverse 90° loading case shown in Figure 10, the model was executed with no changes to the Mat 58 properties shown in Table 1. The model accurately predicted the linear elastic portion of the test response. However, at a strain of 0.005-in/in, the test and predicted responses begin to deviate slightly, with the predicted curve exhibiting the higher magnitude response. The test curve indicates failure at a strain of 0.025-in/in and a stress of 54,000-psi, whereas model failure occurs slightly earlier at a strain of 0.0242-in/in and a slightly higher stress of 54,100-psi. In general, the level of agreement between the test and the predicted response is good. Note that following the maximum strength in the model, the stress is maintained at 43,280-psi, which is the SLIMT2 parameter (0.8) multiplied by the strength of 54,100-psi. This stress level is maintained in the ply until the value of ERODS (0.5) is reached.

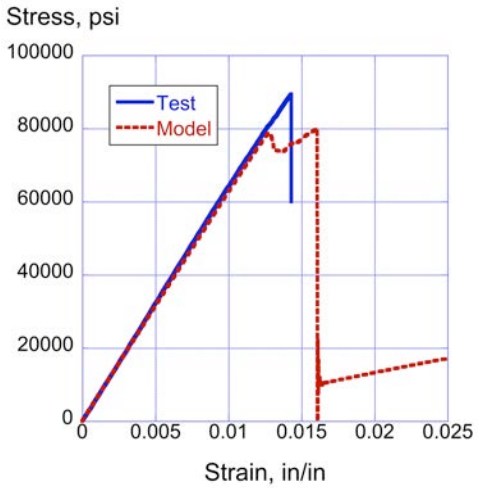


Figure 9. Test-analysis comparison plot of the longitudinal 0° loading case.

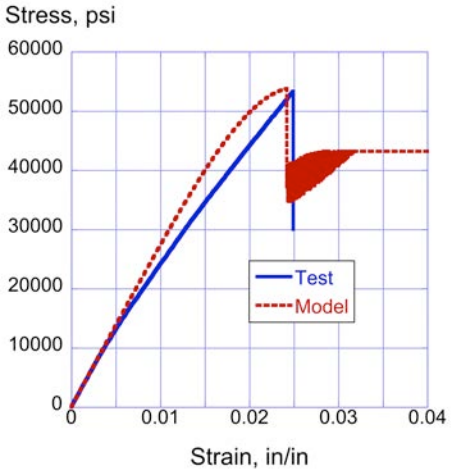


Figure 10. Test-analysis comparison plot of the transverse 90° loading case.

For the ±45° loading results shown in Figure 11, the model was executed with no changes to the Mat 58 properties shown in Table 1. Please note that the curves shown in Figure 11 have not been converted to shear stress and shear strain. At a low strain level, the test and predicted responses begin to deviate. The model exhibits a linear elastic response up to a stress of 8,500 psi. At this point, a sharp "knee" is observed in the response such that it exhibits an elastic-plastic response with strain hardening. The predicted response exhibits a sharp reduction in stress at a strain of 0.105-in/in and a stress of 11,000-psi. Unlike the predicted response, the test curve exhibits a smooth nonlinear response without the sharp knee seen in the predicted response. The test response achieves maximum strength at a strain of 0.188-in/in and a stress of 14,416.0-psi. The early failure of

the model is likely due to complex loading with transverse yielding occurring in one or more plies. In addition, it should be noted that for ±45° coupons loaded in tension, the fibers tend to align with the loading direction as failures occur. However, the model cannot replicate this behavior.

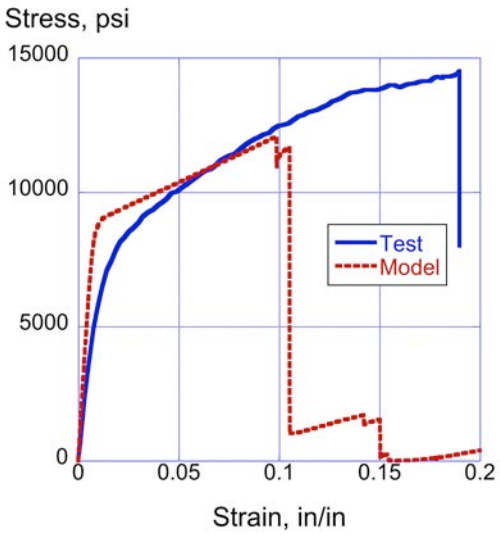


Figure 11. Test-analysis comparison plot of the ±45° loading case.

## IMPACT TESTING AND SIMULATION OF TWO COMPOSITE ENERGY ABSORBERS

Conusoid Energy Absorber

During the development process, different conusoid energy absorber designs were dynamically crushed in a 14-ft. drop tower with an instrumented 110-lb. falling mass. Variations in laminate stacking sequence and material types were considered. The final design configuration utilized the hybrid graphite-Kevlar® plain weave fabric material with a 4-ply laminate stacking sequence of [+45°/-45°/-45°/+45°]. The conusoid component was 7.5-in. tall, 12-in. long, with an overall width of 1.5-in. The conusoid walls were approximately 0.04-in. thick. The impact condition was approximately 264-in/s. The drop mass was instrumented with a 500-g damped accelerometer and data were acquired using a National Instruments Data Acquisition System (DAS) sampling at 25-kHz. Post-processed acceleration data were filtered using a low-pass 4-pole Butterworth filter with a 500-Hz cutoff frequency. A high-speed camera filming at 1-kHz captured the deformation time history, which is depicted in Figure 12. The identified failure mechanism is folding of the conusoid walls, which is a desirable failure mode that produces a constant crush response within the design level of 25-40 g.

A depiction of the finite element model representing the conusoid energy absorber is shown in Figure 13. The model contained 185,940 nodes; 44,294 Belytschko-Tsay shell elements; 116,100 solid elements representing the rigid drop mass, 1 initial velocity card assigned to nodes forming the rigid mass, and 1 body load card defining gravity. The nominal shell element edge length is 0.032-in. The shell elements representing the hybrid graphite-Kevlar® fabric layers were assigned Mat 58, as listed in Table1.

For the conusoid, individual ply layers were input using the *PART_COMPOSITE feature in LS-DYNA® which allows input of ply orientations, ply thicknesses, and ply material designations for each layer within a composite laminate. SPCs were used to constrain the nodes forming the bottom plate. The conusoid model was executed using LS-DYNA® SMP version 971 on a Linux-based workstation with 8 processors and required 11 hours and 49 minutes of clock time to execute the simulation for 0.035-seconds. Model output included time-history responses of the drop mass, and image sequences of structural deformation.

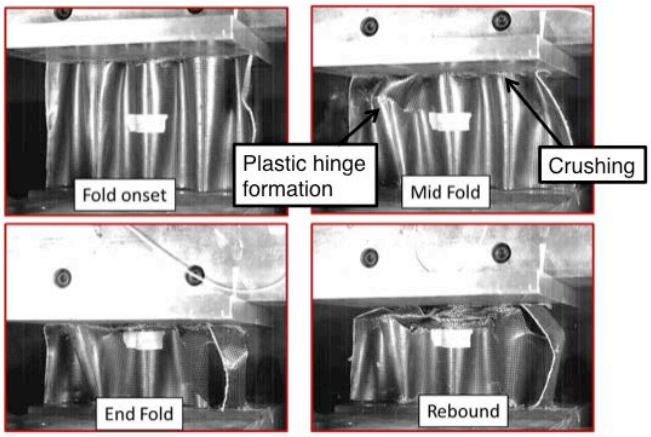


Figure 12. High-speed video clips of conusoid deformation.

Figure 13. Depiction of the conusoid component model.

Comparisons of predicted and experimental acceleration and displacement time histories of the drop mass are shown in Figures 14(a) and (b), respectively. The conusoid model over predicts the magnitude of the initial peak acceleration, 96-g compared with 61-g for the test. However, other than that anomaly, the level of agreement is good. The average acceleration calculated for the test is 28.0-g for pulse duration of 0.0- to 0.025-s, whereas the model average acceleration is 28.4-g for the same duration. The results of the conusoid component test indicate that the configuration of the energy absorber meets all of the design goals,

including achieving a sustained average acceleration level of between 25-40-g. The comparison of vertical displacement time histories also exhibits good agreement, as shown in Figure 14(b). The maximum displacement of the test article is 2.9-in., providing a crush stroke of 38.7%. The maximum displacement of the model is 2.53-in., providing a crush stroke of 33.7%.

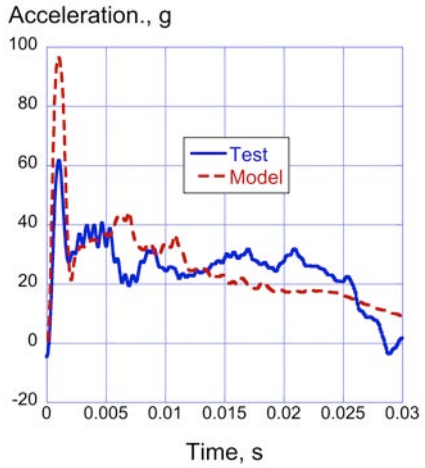


(a) Acceleration responses.

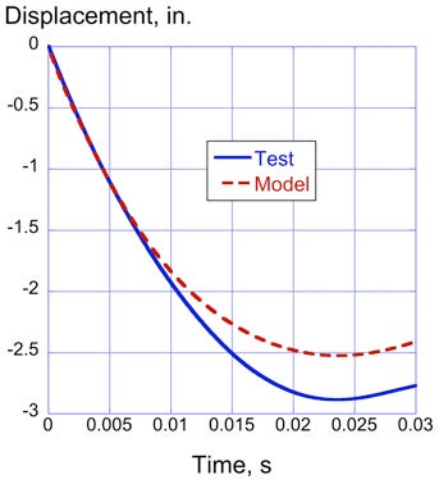


(b) Displacement responses.

Figure 14. Acceleration and displacement comparisons for the conusoid component drop test.

A sequence of model deformation is shown in Figure 15. Stable crushing occurs through plastic hinge formation and folding, along with some local buckling of the conusoid walls. The predicted response is similar to the test deformation captured by the high-speed camera, as shown in Figure 12.

Sinusoid Energy Absorber

The sinusoid foam sandwich energy absorber was initially evaluated through quasi-static and dynamic crush testing of components. Different materials and layups were evaluated for the face sheets; however, the geometry of the sinusoid was not changed since it was based on an existing mold. The final design configuration consisted of hybrid graphite-Kevlar® plain weave fabric face sheets, two layers for each face sheet oriented at ±45° with respect to the vertical or crush direction, and a 1.5-in.-thick closed-cell ELFOAM® P200 polyisocyanurate (2.0-lb/ft$^3$) foam core. The overall width of a sinusoid component was 1.5-in., with a length of 12-in. and a height of 7.5-in. A post-test photograph of a typical sinusoid component is shown in Figure 16 for a dynamic crush test in which a 113.5-lb mass impacted the sinusoid at 265-in/s. A flat 0.5-in.-thick plate was glued to both the top and bottom surfaces of the specimen. As shown in Figure 16, the specimen exhibits stable, plastic-like deformation with uniform folding of the face sheets and crushing of the foam core. Crushing initiates along the top edge of the specimen. Note that the sides of the specimen were not covered with face sheets, which allowed splaying of the foam core.

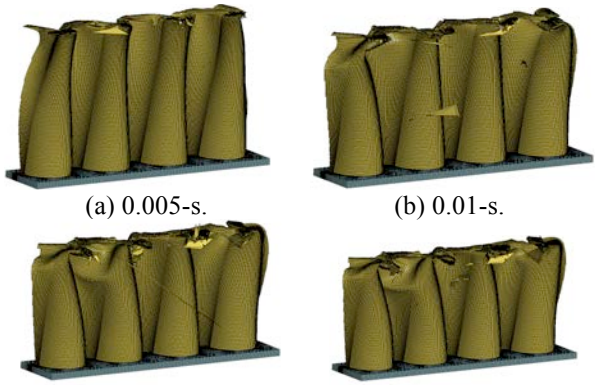

(a) 0.005-s. (b) 0.01-s.

(c) 0.015-s. (d) 0.02-s.

Figure 15. Deformation sequence of the conusoid. Note that deleted elements are highly distorted.

The LS-DYNA® finite element model representing the sinusoid component drop test is shown in Figure 17. The model contained: 53,540 nodes; 7,380 Belytschko-Tsay shell elements; 37,515 solid elements; a rigid drop mass; 1 initial velocity card assigned to nodes forming the rigid drop mass; SPCs to fully constrain the bottom nodes of the sinusoid; 1 automatic single surface contact; and 3 material definitions. As with the conusoid, the shell elements were assigned Mat 58, using the properties listed in Table 1. The nominal element edge length in the sinusoid model was 0.2-inches.

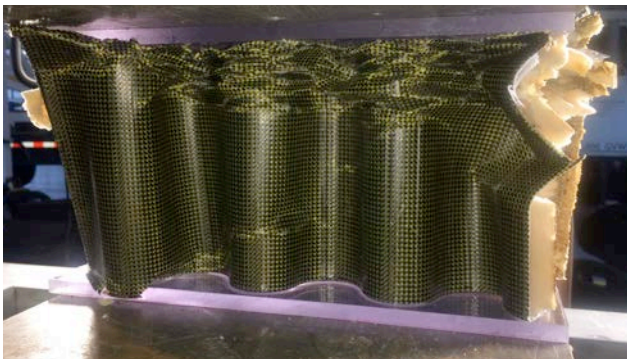

Figure 16. Post-test photograph of a sinusoid foam sandwich energy absorber.

The solid elements representing the foam core were assigned Mat 63, which is a crushable foam material model in LS-DYNA® that allows user input of the stress-strain response of the material in tabular format. The stress-strain response of the P200 foam was determined through quasi-static testing of 4-in. x 4-in. x 3-in. rectangular blocks. A plot of the experimental curve obtained at a crush rate of 1.0-in/minute is shown in Figure 18, along with the stress-strain response used as input to Mat 63. Note that the input curve matches the test data to a strain of 0.67-in/in. At this point, the test data ends, yet the Mat 63 input response continues and increases dramatically up to 100,000-psi at 1-in/in (note that this data point is not shown in the plot). The large "tail" added to the end of the stress-strain response represents compaction of the foam and is needed to stabilize the response of the solid elements for high values of volumetric strain.

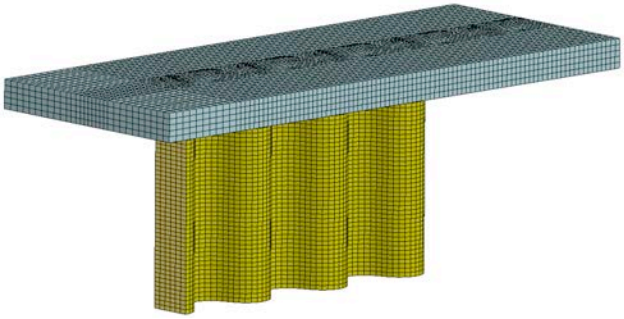

(a) Sinusoid component model.

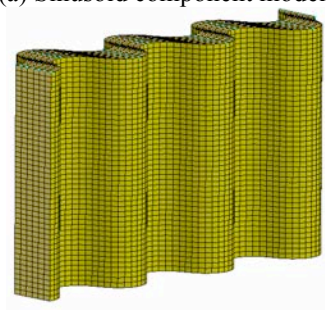

(b) Model without drop mass.

Figure 17. Depictions of the finite element model of the sinusoid component.

The sinusoid model was executed using LS-DYNA® SMP version 971 on a Linux-based workstation with 8 processors and required 10 hours and 34 minutes of clock time to execute the simulation for 0.04-seconds. Model output included time-history responses of the drop mass, and image sequences of structural deformation.

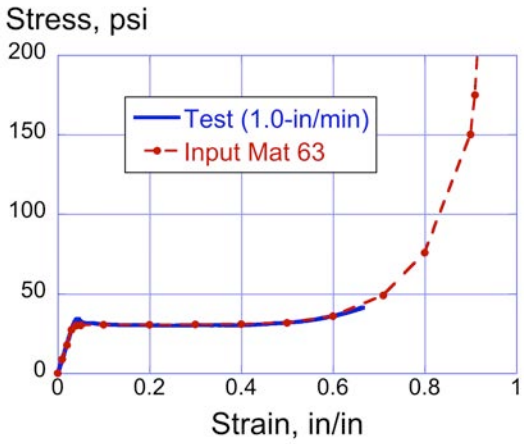


Figure 18. Plot of P200 foam stress-strain response.

Test-analysis comparisons of time-history responses are plotted in Figure 19 for the sinusoid component crush test. These results demonstrate excellent test-analysis agreement. As can be seen in Figure 19(a), the acceleration response of the drop mass achieves an initial peak of 55-g, then drops to approximately 22-g, where it remains constant until the end of the pulse. The model mimics this response, even predicting the unloading response near the end of the pulse. The average acceleration calculated for the test is 21.8-g for pulse duration of 0.0- to 0.03-s, whereas the average acceleration of the predicted response is 22.9-g for the same duration. The experimental and analytical displacement responses, shown in Figure 19(b), exhibit maximum values of 4- and 3.8-in., respectively, which represents approximately 50% stroke. The average acceleration results for the sinusoid fall slightly below the required design range of 25- to 40-g. The lower average crush acceleration for the sinusoid translates into a larger crush stroke than was seen for the conusoid.

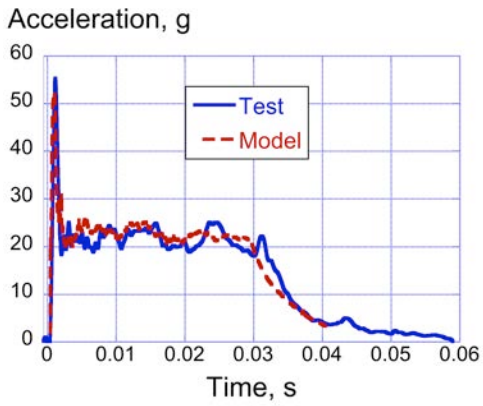


(a) Acceleration responses.

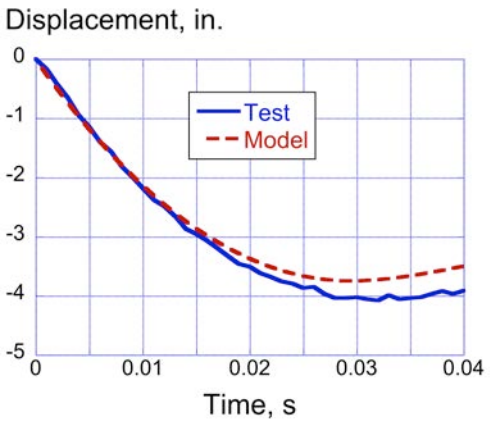


(b) Displacement responses.

Figure 19. Test-analysis time history comparisons for the sinusoid component.

The predicted sinusoid model deformation is shown in Figure 20 for six discrete time steps. The model exhibits stable crushing through folding and plastic-like deformation of the face sheets and crushing of the foam core. The deformation pattern matches the post-test photograph, shown in Figure 16.

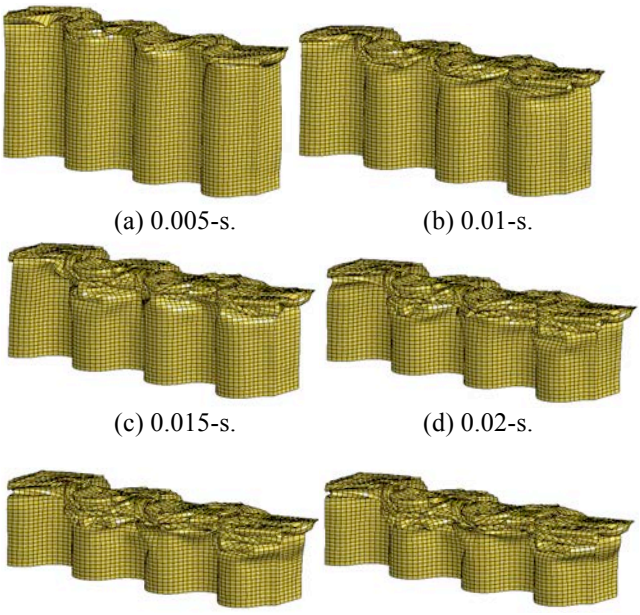

(a) 0.005-s. (b) 0.01-s.

(c) 0.015-s. (d) 0.02-s.

(e) 0.025-s. (f) 0.03-s.

Figure 20. Predicted sinusoid model deformation.

## DISSCUSSION OF RESULTS

In summary, it should be noted that the conusoid energy absorber achieved the design goal of limiting average vertical accelerations to between 25- and 40-g, with an average acceleration of 28.0-g and a crush stroke of 38.7%. The sinusoid energy absorber achieved an average acceleration of 21.8-g, which is below the design range. The lower average acceleration of the sinusoid simply translates into greater crush displacement than seen for the conusoid energy absorber. For example, the crush stoke of the sinusoid energy absorber is approximately 50%.

While the focus of this paper was specifically on the development and application of Mat 58, it should be noted that composite material models are currently being developed to include additional damage mechanisms and rate dependent effects, which may lead to improved predictive capabilities for crash and impact loads in the future. One example is the development of Mat 213 in LS-DYNA®, as described by Goldberg, et al. [17] and Hoffarth et al. [18]. This material model is an orthotropic, elastic-plastic-damage, three-dimensional model based on tabulated input obtained directly from experimental data. Material models, such as Mat 213, do not require input of empirical parameters and are grounded in test data. At this time, Mat 213 has been developed for solid element formulations; however, a shell-based version is under development.

## CONCLUDING REMARKS

A test-analysis study was performed to generate material property data for a hybrid graphite-Kevlar® plain weave fabric for use in a continuum damage mechanics material model, Mat 58, in LS-DYNA®. Material property data were obtained from a limited set of material characterization tests including tensile tests of coupons in which the graphite fibers were oriented in the 0° longitudinal (axial) direction, tensile tests of coupons in which the graphite fibers were oriented in the 90° transverse direction, and tensile tests of coupons in which the graphite fibers were oriented in a ±45° direction. A simple finite element model was executed to simulate the material characterization tests and to verify the Mat 58 material model. Once verified, the Mat 58 model was used in finite element models of two composite energy absorbers: a conical-shaped design, designated the "conusoid," fabricated of four layers of hybrid graphite-Kevlar® fabric; and, a sinusoidal-shaped foam sandwich design, designated the "sinusoid," fabricated of hybrid fabric face sheets, two layers each oriented at ±45°, with a foam core. Dynamic crush tests were performed on the two energy absorbers using a 110-lb drop mass impacting at approximately 265-in/s. Finite element models of the energy absorbers were executed in LS-DYNA® to simulate the dynamic crush tests. Findings are listed, as follows:

- Comparisons between material characterization tests with predicted responses showed reasonable agreement, with the best agreement exhibited by the 90° transverse loading case.

- The conusoid test response had an average acceleration of 28.0-g and maximum crush displacement of 2.9-in., whereas the model exhibited an average acceleration of 28.4-g and a maximum crush displacement of 2.53-in. The simulation did a good job of predicting the conusoid deformation pattern of plastic hinge formation and folding.

- The sinusoid test article exhibited an average acceleration of 21.8-g and a maximum crush displacement of 4.0-inches,

whereas the sinusoid model exhibited an average acceleration of 22.9-g and a maximum crush displacement of 3.8-in. Again, the simulation did an excellent job of predicting the sinusoid deformation pattern of stable crushing through folding and plastic-like deformation of the face sheets and crushing of the foam core.

Finally, the conusoid energy absorber achieved the design goal of limiting average vertical accelerations to between 25- and 40-g, with an average acceleration of 28.0-g and a crush stroke of 38.7%. The sinusoid energy absorber achieved an average acceleration of 21.8-g. The lower average acceleration of the sinusoid simply translates into greater crush displacement than seen for the conusoid energy absorber.

## REFERENCES


[1]Annett M.S., Littell J.D., Jackson K.E., Bark L., DeWeese R., McEntire B.J., "Evaluation of the First Transport Rotorcraft Airframe Crash Testbed (TRACT 1) Full-Scale Crash Test," NASA Technical Memorandum, NASA/TM-2014-218543, October 2014.

[2]Annett M.S., "Evaluation of the Second Transport Rotorcraft Airframe Crash Testbed (TRACT 2) Full Scale Crash Test," Proceedings of the American Helicopter Society International Annual Forum 71, Virginia Beach, VA, May 3-5, 2015.

[3]Kindervater C., Thomson R., Johnson A., David M., Joosten M., Mikulik Z., Mulcahy L., Veldman S., Gunnion A., Jackson A., and Dutton S., "Validation of Crashworthiness Simulation and Design Methods by Testing of a Scaled Composite Helicopter Frame Section," Proceedings of the American Helicopter Society 67th Annual Forum, Virginia Beach, VA, May 3-5, 2011.

[4]Billac T., David M., Battley M., Allen T., Thomson R., Kindervater C., Das R., "Validation of Numerical Methods for Multi-terrain Impact Simulations of a Crashworthy Composite Helicopter Subfloor," Proceedings of the American Helicopter Society 70th Annual Forum, Montreal, Quebec, Canada, May 20-22, 2014.

[5]Littell J. D., "The Development of a Conical Composite Energy Absorber for use in the Attenuation of Crash/Impact Loads," Proceedings of the American Society for Composites 29th Technical Conference, 16th US-Japan Conference on Composite Materials, September 8-10, University of California San Diego, La Jolla, CA.

[6]Jackson K.E., Fasanella E.L., and Littell J.D., "Impact Testing and Simulation of a Sinusoid Foam Sandwich Energy Absorber," Proceedings of the American Society of Composites 30th Technical Conference, East Lansing, MI, September 28-30, 2015.

[7]Hallquist J. O., "LS-DYNA Keyword User's Manual," Volume I, Version 971, Livermore Software Technology Company, Livermore, CA, August 2006.

[8]Hallquist J. O., "LS-DYNA Keyword User's Manual," Volume II Material Models, Version 971, Livermore Software Technology Company, Livermore, CA, August 2006.

[9]Hallquist J. O., "LS-DYNA Theory Manual," Livermore Software Technology Company, Livermore, CA, March 2006.

[10]Jackson K.E., Littell J.D., Fasanella E.L., Annett M.S., and Seal M.D., "Multi-Level Experimental and Analytical Evaluation of Two Composite Energy Absorbers," NASA Technical Memorandum, NASA/TM-2015-218772, July 2015.

[11]Matzenmiller A., Lubliner J., and Taylor R. L., "A Constitutive Model for Anisotropic Damage in Fiber Composites," ***Mechanica of Materials,*** Vol. 20, 1995, pp. 125-152.

[12]Farley G. L., "Energy Absorption of Composite Materials***," Journal of Composite Materials***, 17, (5), May 1983, pp. 267-279.

[13]Carney K., Melis M., Fasanella E., Lyle K., Gabrys J., "Material Modeling of Space Shuttle Leading Edge and External Tank Materials for Use in the Columbia Accident Investigation," 8th International LS-DYNA® Users Conference, Dearborn, MI, May 2-4, 2004, pp. 3-35 through 3-44.

[14]Schweizerhof K., Weimar K., Munz Th., and Rottner, Th., "Crashworthiness Analysis with Enhanced Composite Material Models in LS-DYNA® – Merits and Limits," Proceedings of the 5th International LS-DYNA® Users Conference, Dearborn, Michigan, September 21-22, 1998.

[15]American Society for Testing and Materials, "Standard Test Method for Tensile Properties of Polymer Matrix Composite Materials," ASTM-D3039M, 2008.

[16]American Society for Testing and Materials, "Standard Test Method for In-Plane Shear Response of Polymer Matrix Composite Materials by Tensile Test of a ±45° Composite," ASTM D3518M, 2013.

[17]Goldberg R.K., Carney K. S., DuBois P., Hoffarth C., Khaled B., Rajan, S., and Blankenhorn G., "Incorporation of damage and failure into an orthotropic elasto-plastic three-dimensional model with tabulated input suitable for use in composite impact problems," Proceedings of the 14th International LS-DYNA Users Conference, Dearborn, MI, 2016.

[18]Hoffarth C., Khaled B., Rajan S.D., Goldberg R., Carney K., DuBois P., Blankenhorn G., "Using tabulated experimental data to drive an orthotropic elasto-plastic three-dimensional model for impact analysis," Proceedings of the 14th International LS-DYNA Users Conference. Dearborn, MI, 2016.

Author contact:

1. Karen Jackson, Karen.E.Jackson-1@nasa.gov

2. Edwin Fasanella, edfas1@verizon.net.

3. Justin Littell, Justin.D.Littell@nasa.gov